Polarization Singularities of Photonic Quasicrystals in Momentum Space

Zhiyuan Che,[1] Yanbin Zhang,[1] Wenzhe Liu,[1] Maoxiong Zhao,[1] Jiajun Wang,[1] Wenjie Zhang,[1] Fang Guan,[1] Xiaohan Liu,[1] Wei Liu,[2] Lei Shi,[1,3,*] and Jian Zi[1,3,†]

[1]*State Key Laboratory of Surface Physics, Key Laboratory of Micro- and Nano-Photonic Structures (Ministry of Education) and Department of Physics, Fudan University, Shanghai 200433, China*

[2]*College for Advanced Interdisciplinary Studies, National University of Defense Technology, Changsha, Hunan 410073, China*

[3]*Collaborative Innovation Center of Advanced Microstructures, Nanjing University, Nanjing 210093, China*

(Received 27 February 2021; accepted 22 June 2021; published 22 July 2021)

We report the observation of polarization singularities in momentum space of 2D photonic quasicrystal slabs. Supercell approximation and band-unfolding approach are applied to obtain approximate photonic dispersions and the far-field polarization states defined on them. We discuss the relations between the topological charges of the polarization vortex singularities at Γ points and the symmetries of photonic quasicrystal slabs. With a perspective of multipolar expansions for the supercell, we confirm that the singularities are protected by the point-group symmetry of the photonic quasicrystal slab. We further uncover that the polarization singularities of photonic quasicrystal slab correspond to quasibound states in the continuum with exceptionally high-quality factors. Polarization singularities of different topological charges are also experimentally verified. Our Letter introduces core concepts of optical singularities into quasiperiodic systems, providing new platforms for explorations merging topological and singular optics.

DOI: 10.1103/PhysRevLett.127.043901

Largely fueled by the recent explosive developments of nanophotonics and its related disciplines of topological and/or non-Hermitian photonics [1–7], optical singularities [8–11] (singularities of phase and polarizations, in particular [12–20]) have rapidly pervaded various branches of photonics. Through the unique perspective of singularities, subtle connections have been established among a wide range of fundamental concepts, including but not limited to electromagnetic multipoles [20,21], bound states in the continuum (BICs) [22–27], geometric phase [28–31], topological charge conservation [16,18,30], non-Hermitian degeneracies [6,30,32,33], and optical chirality [34,35], which renders broader and deeper insights into many exotic optical phenomena. Unfortunately, so far along the line to exploit optical singularities together with other fundamental concepts has been implemented mainly in periodic photonic crystals, the functionalities of which are severely constrained by their limited rotational symmetry (sixfold at most) and the thus induced optical anisotropy. It is rather natural to expect that further extensions from periodic to quasiperiodic systems, exhibiting both long-range order and unlimited rotational symmetry [36–50], would not only help to surmount the aforementioned obstacles, but also open up new vistas in further explorations into singularity-related light matter interactions.

In this Letter, the polarization singularities on the photonic dispersions of 2D photonic quasicrystal (PQC) slabs are reported. These singularities, where the intensity of far field vanishes (referred to as *V* points), are the centers of polarization vortices in momentum space. Because of the high rotational symmetry of quasicrystals, singularities with high-order topological charges are observed both theoretically and experimentally. The fundamental concepts we discuss in this Letter (singularity, topology, and quasiperiodicity) are not exclusive or confined to photonics only, but are rather pervasive in many other disciplines and, in particular, condensed matter physics.

We first study the eigenmodes and photonic dispersions of PQC slabs, applying the supercell calculation and band-unfolding approach [45,51–54]. The supercell containing quasicrystal fragments is obtained from rational periodic approximants of quasicrystals [55–57]. A square-shaped supercell of the second-order approximation of an eightfold PQC slab is shown in Fig. 1(a) (see Supplemental Material [58]). Its Fourier transform (FT) pattern exhibits similar diffraction patterns to those of ideal quasicrystal, as shown in Fig. 1(b). In the periodic approximation of quasicrystals, there are two sets of reciprocal lattice vectors. The first one is the reciprocal lattice vectors of the supercell, defined as $\mathbf{G}_{nm} = n\mathbf{B}_1 + m\mathbf{B}_2$, where $\mathbf{B}_1$ and $\mathbf{B}_2$ are the reciprocal lattice basis vectors of the periodic square-shaped supercell structure, and n and m are arbitrary integers. The other one is the reciprocal lattice vector of the quasicrystal structure, denoted as $\mathbf{g}$. Note that the formed set $\{\mathbf{g}\}$ is a subset of $\{\mathbf{G}_{nm}\}$. As an example, for an eightfold rotational quasicrystal with a square-shaped supercell, its basic set of vectors $\mathbf{g}$ is shown in Fig. 1(b), denoted as $\{\mathbf{b}_i; i = 1, 2, 3, 4\}$. For the second-order approximation, these basis vectors can be identified as $\mathbf{b}_1 = \mathbf{G}_{70}$, $\mathbf{b}_2 = \mathbf{G}_{07}$, $\mathbf{b}_3 = \mathbf{G}_{55}$, and $\mathbf{b}_4 = \mathbf{G}_{-55}$. Thus, an octagon in

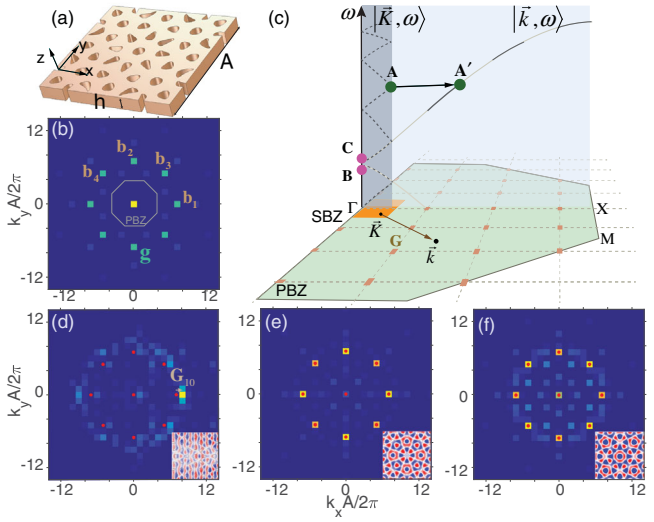

FIG. 1. Band unfolding of PQC slab through supercell approximation. (a),(b) Supercell of eightfold PQC slab and Fourier transform pattern. (c) Schematic view of band unfolding. The bands (dotted lines) in supercell BZ are unfolded into pseudo-BZ bands. (d)–(f) Unfolding examples of computed modes marked as dots **A**–**C** in (c).

reciprocal space is defined as the pseudo-BZ (PBZ) of an eightfold quasicrystal [56], as shown in Fig. 1(b). Here the half of PBZ is indicated as the green zone in Fig. 1(c). In Fig. 1(c), the first Brillouin zone of the supercell (SBZ) is also indicated as the orange zone. The wave vectors inside the PBZ (SBZ) are denoted by $\vec{k}(\vec{K})$ and they obey the relation $\vec{k} = \vec{K} + \mathbf{G}_{nm}$ for the geometric symmetry of two Brillouin zones. The eigenmodes $|\vec{K}, \omega\rangle$ obtained from the supercell calculation can construct band structure $\omega(\vec{K})$. To get the approximate dispersion of quasicrystal $\omega(\vec{k})$, the band-unfolding approach is used to project the SBZ bands onto PBZ.

In Fig. 1(c), we show the schematic views of the unfolding process of SBZ bands. According to the Bloch theorem for photonic crystals, the wave function of eigenmode $|\vec{K}, \omega\rangle$ on the SBZ bands can be written as $\mathbf{u}_{\vec{K}}(\mathbf{r})e^{i\vec{K}\cdot\mathbf{r}}$, where $\mathbf{u}_{\vec{K}}$ possesses the spatial periodicity and can be expanded in Fourier series. Meanwhile, the $\mathbf{u}_{\vec{K}}$ within a single supercell possesses the features of the PQC slab and the corresponding FT pattern will have similar diffraction spots as that of the supercell structure. When these diffraction spots of the FT pattern of $\mathbf{u}_{\vec{K}}$ are exactly overlapping with the $\mathbf{g}$ vectors, this mode can be approximated to the eigenmode of the quasicrystals and can be mapped onto the PBZ at $\vec{k} = \vec{K}$ with the same frequency; when these diffraction spots are not overlapping with the $\mathbf{g}$ vectors, a proper $\mathbf{G}_{nm}$ needs to be found to unfold this mode onto the PBZ. Actually, this mode can be rewritten as $\tilde{\mathbf{u}}_{(\vec{K}+\mathbf{G}_{nm})}(\mathbf{r})e^{i(\vec{K}+\mathbf{G}_{nm})\cdot\mathbf{r}}$ with a vector $\mathbf{G}_{nm}$, where $\tilde{\mathbf{u}}_{(\vec{K}+\mathbf{G}_{nm})} = \mathbf{u}_{\vec{K}}(\mathbf{r})e^{-i\mathbf{G}_{nm}\cdot\mathbf{r}}$. Once the FT pattern of $\tilde{\mathbf{u}}_{(\vec{K}+\mathbf{G}_{nm})}$ for a certain $\mathbf{G}_{nm}$ has diffraction spots overlapping with the $\mathbf{g}$ vectors, this suggests that the mode $|\vec{K}, \omega\rangle$ lain in SBZ possesses Bloch character $\vec{k} = \vec{K} + \mathbf{G}_{nm}$ and can be represented as $|\vec{k}, \omega\rangle$. Specifically, some unfolding examples of the calculated modes marked as dots **A**–**C** in Fig. 1(c) are shown. The structure parameters of a square lattice supercell of an eightfold PQC slab are as follows: lattice constant $A = 7a$, $a = 0.48$ μm, thickness $h = 0.1$ μm, and refractive index $n = 2.0$ with filling ratio 0.79. For a mode at the boundary of SBZ (dot **A**), its FT pattern is shown in Fig. 1(d), and its corresponding field profile is plotted in the bottom-right corner. We can find one dominant diffraction spot on this pattern and can overlap with the $\mathbf{g}$ vectors by shifting one unit to the left. Thus, this mode should be unfolded into $|\vec{K} + \mathbf{G}_{10}, \omega\rangle$, indicated in Fig. 1(c) as from **A** to **A**′. For an at-Γ mode, its FT pattern shows eight diffraction spots overlapping with $\mathbf{g}$ vectors, as plotted in Fig. 1(e). So $\mathbf{G}_{nm} = 0$ and $\vec{k} = 0$. This mode should reserve at Γ point, as dot **B** marked in the schematic band in Fig. 1(c). Figure 1(f) is similar to Fig. 1(e), except for a mode of another band (dot **C**). When repeating the unfolding of thousands of SBZ eigenmodes, we will obtain the dispersion of quasicrystals in the PBZ.

In Fig. 2(a), the unfolded dispersions of TM-like modes for 2D eightfold PQC slab are plotted. Compared to the model of empty-lattice approximation [61], the band-unfolding scheme through the supercell calculation not only can be applied to the PQC in high index contrast, but also shows great potential for revealing various photonic properties including the band gap and the far-field polarization states of the radiation mode. This approach will become a powerful and generic method for investigations of PQCs. Subsequently, we would obtain the projected polarization field on these PQC slab dispersions. The polarization field is defined by collecting the far-field polarization state of each radiation mode on one specified band (or dispersion) and mapping the projected polarization states on the $x - y$ plane onto the momentum space [13,16,19]. The polarization maps near the Γ point of TM-like dispersions [−1000] and [1000] are plotted in Fig. 2(b). We can see that the vortex polarization singularities (V points) appear in the center of vortex fields. The carried topological charges are $+1$ and -3, corresponding to the left and right panel of Fig. 2(b), respectively. To deeply understand the topological properties of the polarization singularities, symmetry analyses in both momentum and real spaces are shown below.

To begin with, we use the group theory to analyze the relations between the topological charges of polarization vortex in the vicinity of the Γ point and the symmetry of the eightfold PQC slabs in the momentum space. At the Γ point, its point group is C_{8v}. Thus, there are two singly degenerate modes and six doubly degenerate modes for the

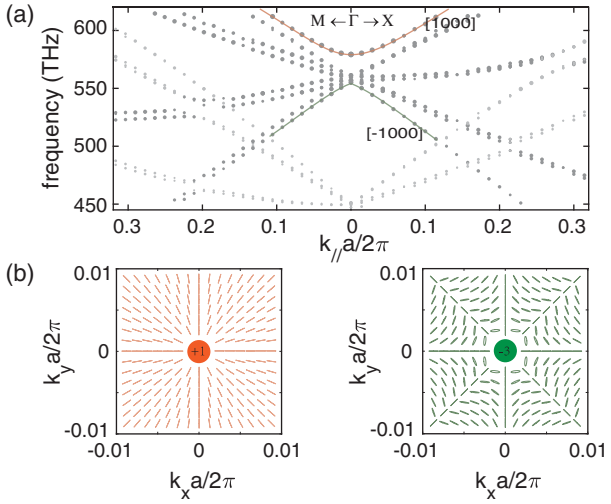

FIG. 2. Unfolded dispersions and polarization maps of an eightfold PQC slab. (a) TM-like dispersions. (b) Polarization maps near the Γ point of TM-like dispersions [−1000] and [1000].

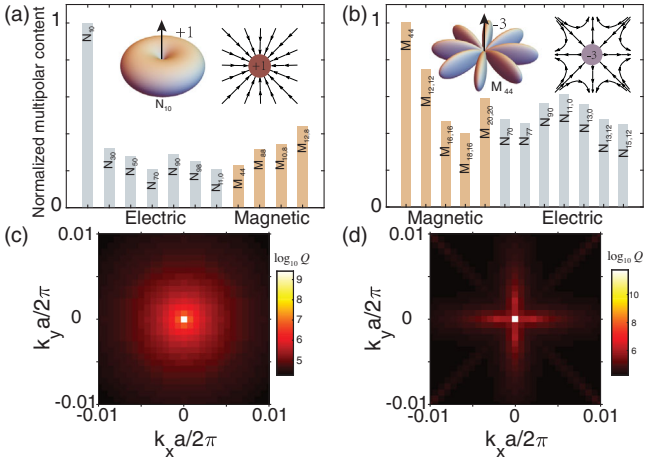

FIG. 3. Multipolar contents of TM-like modes: (a) A_1 and (b) B_1. The far-field radiation and vector field pattern of major multipoles are shown in insets. (c),(d) Simulated quality factor (Q) maps of TM-like modes near the Γ point.

first scattering order. Both doubly degenerate modes and singly degenerate modes would correspond to the vortex polarization singularities, where the far-field polarization is undetermined or undefinable [32,33]. The possible topological charges at high-symmetry points can be determined by the directions of those polarization vectors on the mirror-invariant momentum lines surrounding the high-symmetry point [15]. For the 2D eightfold rotational PQC slab, there are eight mirror-invariant lines in the PBZ intersecting at the Γ point. On these high-symmetry lines, the far-field polarization state is liner polarized, and the projected polarization vector would be either parallel or perpendicular to these lines. By exhausting all possible combinations of the projected polarization vectors on these high-symmetry lines, all possible topological charges at Γ point are $8n+1$ and $8n-3$ with an integer n. Specifically, for $8n+1$ charges, the projected polarization vectors will be synchronously parallel or perpendicular to these adjacent high-symmetry lines. But for $8n-3$ charges, the projected polarization vectors will be one parallel, while another one is perpendicular to two adjacent lines. The configurations of polarization vortices around the high-symmetry point in the case of $n=0$ are shown in Table S1 of the Supplemental Material [58].

The topological properties of these polarization singularities not only can be revealed from the polarization states around the high-symmetry point, but also can be analyzed from the multipolar radiation of near-field displacement currents of the corresponding modes. With the perspective of multipolar radiation, the V points or BICs of photonic crystal slabs have been interpreted as overlapping of radiation singularities on the momentum sphere of the unit cell with specific open channel [21,62]. The assigned Poincaré index of each radiation singularity is essentially equivalent to the topological charge of the polarization vortex [21]. Especially, the index of singularities along the z direction (perpendicular to the structure plane) can be obtained directly by azimuthal quantum number m of multipoles, $1-|m|$. We thus employ the multipolar expansion to the singly degenerate modes corresponding to the V points with $8n+1$ and $8n-3$ charges. These modes are, respectively, transformed according to the A_1 and B_1 irreducible representations of C_{8v}. The expansion coefficients that correspond to electric and magnetic multipoles are carried out by the near-field displacement currents within the supercell. The radiated fields of multipoles are characterized by vector spherical harmonics $\mathbf{M}_{lm}$ and $\mathbf{N}_{lm}$ [63,64]. Figure 3(a) shows the dominant multipolar components of the TM-like A_1 mode and Fig. 3(b) shows that of the B_1 mode. Other minor multipoles are not shown, without affecting the following conclusion. For both A_1 and B_1 modes, it is certain that all nonzero multipolar components have radiation singularities along the z direction. The major dominant multipole of A_1 mode is $\mathbf{N}_{10}$, and its index of singularity along the z direction is $+1$. For the B_1 mode, the major dominant multipole is $\mathbf{M}_{4,\pm4}$, and its index of singularity is -3. (See Supplemental Material [58] for a detailed discussion of the existence of high-order multipoles.) These indexes are consistent with the topological charge of the polarization vortex. The corresponding vector field patterns close to singularities present similar vortex configurations to polarization maps shown in Fig. 2.

To further understand the radiation singularities of the PQC slabs, we turn to ideal quasicrystal without the periodic approximation. We will show that the radiation singularities are protected by the symmetries of quasicrystal displayed in real space. To describe the ideal quasicrystals in the real space, the cluster model has been

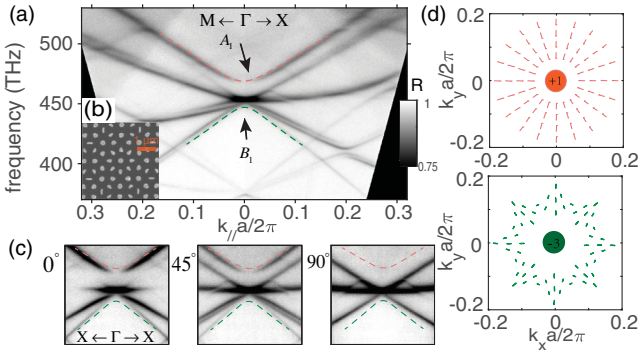

FIG. 4. (a) Measured dispersions for a plasmonic quasicrystal structure, with its SEM image shown in (b). (c) Polarization-dependent reflectance spectrum of SPP modes. (d) Polarization maps extracted from the polarization-resolved spectrum.

proposed to view the local cluster as the building blocks of quasicrystal structures [65–67]. The local clusters of an eightfold PQC slab occupy an octagon that possesses symmetries of C_{8v} (see Supplemental Material [58]). We now apply the group-symmetry approach [68–72] to analyze the multipolar radiation of the local cluster of the PQC slab. First and foremost, due to the highest rotational operation being C_8^z for the local cluster, the multipoles with $m = \pm 1$, which only satisfy the C_2 rotational symmetry, are not allowed for the mode with A_1 or B_1 irreducible representations. These multipoles $\mathbf{M}_{l,\pm 1}$ ($\mathbf{N}_{l,\pm 1}$) are the only radiative content along the z direction. Specifically, on the constrains of reflection and rotational operations, all possible multipolar components are classified in accordance with two irreducible representations in Table S1 of the Supplemental Material [58]. The lowest-order multipole of mode A_1 and mode B_1 is $\mathbf{N}_{10}$ and $\mathbf{M}_{4,\pm 4}$, respectively, which is consistent with the results of multipolar expansion of near-field displacement currents within the supercell summarized in Fig. 3. In virtue of the symmetry analyses, we conclude that the radiation singularities along the z direction of two singly degenerate modes at Γ point are guaranteed by the C_{8v} symmetry. Although we focused on the eightfold PQC slabs here, the same discussions can be extended to other systems, such as 10- and 12-fold rotational PQC slabs.

Based on group-symmetry analyses and multipolar expansion, the existence of radiation singularities along the z direction confirmed that the polarization singularities of PQC slabs are an inevitable result of point-group symmetry and seems to predict that those polarization singularities at the Γ point will also be BICs, as in periodic photonic crystals [12–16,21–27]. Nevertheless, unlike the finite radiation channels of modes of periodic structures that corresponds to diffractions channels of different orders along certain directions, the modes of the PQC slab actually have countless outgoing channels for the absence of translational symmetry, even though all the main radiation channels are limited to a small range for the relatively sharp peaks in the diffraction pattern of the PQC slab. As a result, the electromagnetic energy of the PQC slab mode will partially leak out to the free space from channels around the singularities. Therefore, in contrast to the periodic scenario, the polarization singularity of the PQC slab at the Γ point would be quasi-BICs, i.e., leaky mode with high-quality factor (Q). The simulated Q maps, plotted in Figs. 3(c) and 3(d) for the TM-like A_1 and B_1 modes, show the corresponding quasi-BICs of which the Q tend to infinity when considering only the zero-order channel. Obviously, the presence of other radiation channels would reduce the actual Q.

For an experimental observation of those phenomena, we fabricate plasmonic quasicrystals to verify theoretical analyses. The plasmonic quasicrystals are poly(methylmethacrylate) thin film with the quasicrystals pattern fabricated using electron-beam lithography coating on the flat silver film. We applied our homemade momentum-space imaging spectroscopy system to obtain their angle-resolved reflectance spectrum, as shown in Fig. 4(a) with their SEM image in Fig. 4(b). The spectrum shows the existence of a diminishing point at the Γ point. The disappearance indicates that those modes are hardly to be excited and are nearly decoupled from the free space. Considering that the behavior of the surface plasmon polaritons (SPPs) at the metal-dielectric interface is similar to the lowest TM-like guided modes, we can compare the measured polarization state fields with the TM-like simulated polarization maps. By changing the orientation of the analyzer to 0°, 45°, and 90° relative to the direction of the entrance slit of the spectrometer, we measured polarization-dependent reflectance spectrum of SPP modes and extracted the polarization state from them using the temporal coupled mode theory analyses [15,17]. The extracted polarization state fields are plotted in Fig. 4(d). We can directly see vortex configurations around the quasi-BICs and the topological charges are coincident with the theoretical and simulated results. It is worth mentioning that higher topological charges are more accessible in quasicrystals that are not limited by sixfold rotation symmetry. For example, we have indeed observed a charge of −5 in 12-fold rotational plasmonic quasicrystals, as shown in Fig. S11 in the Supplemental Material [58]. Similar phenomena can be observed in the PQC slabs (see details in the Supplemental Material [58]). In addition, various polarization singularities also exist in the degenerate bands at the Γ point, see Fig. S7 [58].

In conclusion, we have theoretically verified and experimentally observed the existence of the polarization singularities of 2D quasicrystal structures with high-rotational symmetry. Our Letter shows that the polarization singularities in the momentum space do not depend on the translational symmetry, but the point-group symmetry plays a key role in topological polarization properties of photonic structures. Sole rotational symmetry of quasicrystals can generate polarization singularities of charges that

are inaccessible in their periodic counterparts, which may provide extra freedom for various singularity-related optical applications, including generation of higher charges vortex beam [27] and topological vortex microlaser [73,74]. In addition to higher charges, rich degeneracies at the Γ point are another fundamental advantage from high-rotational symmetry of quasicrystals. With the further introduction of topological concepts, quasicrystals may be a versatile platform for observing various topological phenomenons, such as non-Abelian geometric phases [28,29,31], non-Hermitian effects [6,30,32], and high-order topological phases [75,76].

The work was supported by the China National Key Basic Research Program (2016YFA0301103, 2016YFA0302000, and 2018YFA0306201) and the National Science Foundation of China (11774063, 11727811, 91963212, and 11874426). L. S. was further supported by the Science and Technology Commission of Shanghai Municipality (19XD1434600, 2019SHZDZX01, and 19DZ2253000). We thank Professor Yuntian Chen and Dr. Weijin Chen for help with our multipolar expansion calculations.

*lshi@fudan.edu.cn
†jzi@fudan.edu.cn

[1] A. B. Khanikaev, S. H. Mousavi, W.-K. Tse, M. Kargarian, A. H. MacDonald, and G. Shvets, Photonic topological insulators, Nat. Mater. **12**, 233 (2013).
[2] L. Lu, J. D. Joannopoulos, and M. Soljai, Topological photonics, Nat. Photonics **8**, 821 (2014).
[3] L. Feng, R. El-Ganainy, and L. Ge, Non-Hermitian photonics based on parity–time symmetry, Nat. Photonics **11**, 752 (2017).
[4] A. B. Khanikaev and G. Shvets, Two-dimensional topological photonics, Nat. Photonics **11**, 763 (2017).
[5] B. Midya, H. Zhao, and L. Feng, Non-Hermitian photonics promises exceptional topology of light, Nat. Commun. **9**, 2674 (2018).
[6] M.-A. Miri and A. Al, Exceptional points in optics and photonics, Science **363**, eaar7709 (2019).
[7] H. Zhao, X. Qiao, T. Wu, B. Midya, S. Longhi, and L. Feng, Non-Hermitian topological light steering, Science **365**, 1163 (2019).
[8] M. V. Berry, *A Half-Century of Physical Asymptotics and Other Diversions: Selected Works by Michael Berry* (World Scientific, Singapore, 2017).
[9] M. R. Dennis, K. O'Holleran, and M. J. Padgett, Singular optics: Optical vortices and polarization singularities, in *Progress in Optics*, edited by E. Wolf (Elsevier, New York, 2009),Vol. 53, Chap. 5, pp. 293–363.
[10] Y. Shen, X. Wang, Z. Xie, C. Min, X. Fu, Q. Liu, M. Gong, and X. Yuan, Optical vortices 30 years on: OAM manipulation from topological charge to multiple singularities, Light Sci. Appl. **8**, 90 (2019).
[11] W. Liu, W. Liu, L. Shi, and Y. Kivshar, Topological polarization singularities in metaphotonics, Nanophotonics **10**, 1469 (2020).
[12] C. W. Hsu, B. Zhen, J. Lee, S.-L. Chua, S. G. Johnson, J. D. Joannopoulos, and M. Soljačić, Observation of trapped light within the radiation continuum, Nature (London) **499**, 188 (2013).
[13] B. Zhen, C. W. Hsu, L. Lu, A. D. Stone, and M. Soljačić, Topological Nature of Optical Bound States in the Continuum, Phys. Rev. Lett. **113**, 257401 (2014).
[14] H. M. Doeleman, F. Monticone, W. den Hollander, A. Al, and A. F. Koenderink, Experimental observation of a polarization vortex at an optical bound state in the continuum, Nat. Photonics **12**, 397 (2018).
[15] Y. Zhang, A. Chen, W. Liu, C. W. Hsu, B. Wang, F. Guan, X. Liu, L. Shi, L. Lu, and J. Zi, Observation of Polarization Vortices in Momentum Space, Phys. Rev. Lett. **120**, 186103 (2018).
[16] W. Ye, Y. Gao, and J. Liu, Singular Points of Polarizations in the Momentum Space of Photonic Crystal Slabs, Phys. Rev. Lett. **124**, 153904 (2020).
[17] W. Liu, B. Wang, Y. Zhang, J. Wang, M. Zhao, F. Guan, X. Liu, L. Shi, and J. Zi, Circularly Polarized States Spawning from Bound States in the Continuum, Phys. Rev. Lett. **123**, 116104 (2019).
[18] X. Yin, J. Jin, M. Soljačić, C. Peng, and B. Zhen, Observation of topologically enabled unidirectional guided resonances, Nature (London) **580**, 467 (2020).
[19] T. Yoda and M. Notomi, Observation of topologically enabled unidirectional guided resonances, Phys. Rev. Lett. **125**, 053902 (2020).
[20] W. Chen, Y. Chen, and W. Liu, Line singularities and hopf indices of electromagnetic multipoles, Laser Photonics Rev. **14**, 2000049 (2020).
[21] W. Chen, Y. Chen, and W. Liu, Singularities and Poincaré Indices of Electromagnetic Multipoles, Phys. Rev. Lett. **122**, 153907 (2019).
[22] Y. Yang, C. Peng, Y. Liang, Z. Li, and S. Noda, Analytical Perspective for Bound States in the Continuum in Photonic Crystal Slabs, Phys. Rev. Lett. **113**, 037401 (2014).
[23] C. W. Hsu, B. Zhen, A. D. Stone, J. D. Joannopoulos, and M. Soljačić, Bound states in the continuum, Nat. Rev. Mater. **1**, 16048 (2016).
[24] E. N. Bulgakov and D. N. Maksimov, Bound states in the continuum and polarization singularities in periodic arrays of dielectric rods, Phys. Rev. A **96**, 063833 (2017).
[25] K. Koshelev, S. Lepeshov, M. Liu, A. Bogdanov, and Y. Kivshar, Asymmetric Metasurfaces with High-Q Resonances Governed by Bound States in the Continuum, Phys. Rev. Lett. **121**, 193903 (2018).
[26] J. Jin, X. Yin, L. Ni, M. Soljačić, B. Zhen, and C. Peng, Topologically enabled ultrahigh-Q guided resonances robust to out-of-plane scattering, Nature (London) **574**, 501 (2019).
[27] B. Wang, W. Liu, M. Zhao, J. Wang, Y. Zhang, A. Chen, F. Guan, X. Liu, L. Shi, and J. Zi, Generating optical vortex beams by momentum-space polarization vortices centred at bound states in the continuum, Nat. Photonics **14**, 623 (2020).

[28] Y. Yang, C. Peng, D. Zhu, H. Buljan, J. Joannopoulos, B. Zhen, and M. Soljačić, Synthesis and observation of non-Abelian gauge fields in real space, Science **365**, 1021 (2019).
[29] Y. Chen, R.-Y. Zhang, Z. Xiong, Z. Hang, J. Li, J. Shen, and C. T. Chan, Non-Abelian gauge field optics, Nat. Commun. **10**, 3125 (2019).
[30] W. Chen, Q. Yang, Y. Chen, and W. Liu, Evolution and global charge conservation for polarization singularities emerging from non-Hermitian degeneracies, Proc. Natl. Acad. Sci. U.S.A. **118**, e2019578118 (2021).
[31] X. Xie, M. Pu, J. Jin, M. Xu, Y. Guo, X. Li, P. Gao, X. Ma, and X. Luo, Generalized Pancharatnam-Berry Phase in Rotationally Symmetric Meta-Atoms, Phys. Rev. Lett. **126**, 183902 (2021).
[32] H. Zhou, C. Peng, Y. Yoon, C. W. Hsu, K. A. Nelson, L. Fu, J. D. Joannopoulos, M. Soljačić, and B. Zhen, Observation of bulk Fermi arc and polarization half charge from paired exceptional points, Science **359**, 1009 (2018).
[33] A. Chen, W. Liu, Y. Zhang, B. Wang, X. Liu, L. Shi, L. Lu, and J. Zi, Observing vortex polarization singularities at optical band degeneracies, Phys. Rev. B **99**, 180101(R) (2019).
[34] M. V. Berry and M. R. Dennis, Observing vortex polarization singularities at optical band degeneracies, Proc. R. Soc. A **459**, 1261 (2003).
[35] W. Chen, Q. Yang, Y. Chen, and W. Liu, Extremize Optical Chiralities through Polarization Singularities, Phys. Rev. Lett. **126**, 253901 (2021).
[36] Y. S. Chan, C. T. Chan, and Z. Y. Liu, Photonic Band Gaps in Two Dimensional Photonic Quasicrystals, Phys. Rev. Lett. **80**, 956 (1998).
[37] M. E. Zoorob, M. D. B. Charlton, G. J. Parker, J. J. Baumberg, and M. C. Netti, Complete photonic bandgaps in 12-fold symmetric quasicrystals, Nature (London) **404**, 740 (2000).
[38] M. Bayindir, E. Cubukcu, I. Bulu, and E. Ozbay, Photonic band-gap effect, localization, and waveguiding in the two-dimensional Penrose lattice, Phys. Rev. B **63**, 161104(R) (2001).
[39] M. Notomi, H. Suzuki, T. Tamamura, and K. Edagawa, Lasing Action due to the Two-Dimensional Quasiperiodicity of Photonic Quasicrystals with a Penrose Lattice, Phys. Rev. Lett. **92**, 123906 (2004).
[40] A. Della Villa, S. Enoch, G. Tayeb, V. Pierro, V. Galdi, and F. Capolino, Band Gap Formation and Multiple Scattering in Photonic Quasicrystals with a Penrose-Type Lattice, Phys. Rev. Lett. **94**, 183903 (2005).
[41] Z. Feng, X. Zhang, Y. Wang, Z.-Y. Li, B. Cheng, and D.-Z. Zhang, Negative Refraction and Imaging Using 12-fold-Symmetry Quasicrystals, Phys. Rev. Lett. **94**, 247402 (2005).
[42] R. Lifshitz, A. Arie, and A. Bahabad, Photonic Quasicrystals for Nonlinear Optical Frequency Conversion, Phys. Rev. Lett. **95**, 133901 (2005).
[43] W. Steurer and D. Sutter-Widmer, Photonic and phononic quasicrystals, J. Phys. D **40**, R229 (2007).
[44] M. C. Rechtsman, H.-C. Jeong, P. M. Chaikin, S. Torquato, and P. J. Steinhardt, Optimized Structures for Photonic Quasicrystals, Phys. Rev. Lett. **101**, 073902 (2008).
[45] M. Florescu, S. Torquato, and P. J. Steinhardt, Complete band gaps in two-dimensional photonic quasicrystals, Phys. Rev. B **80**, 155112 (2009).
[46] L. Jia, I. Bita, and E. L. Thomas, Impact of Geometry on the TM Photonic Band Gaps of Photonic Crystals and Quasicrystals, Phys. Rev. Lett. **107**, 193901 (2011).
[47] Z. V. Vardeny, A. Nahata, and A. Agrawal, Optics of photonic quasicrystals, Nat. Photonics **7**, 177 (2013).
[48] J.-W. Dong, M.-L. Chang, X.-Q. Huang, Z. H. Hang, Z.-C. Zhong, W.-J. Chen, Z.-Y. Huang, and C. T. Chan, Conical Dispersion and Effective Zero Refractive Index in Photonic Quasicrystals, Phys. Rev. Lett. **114**, 163901 (2015).
[49] M. A. Bandres, M. C. Rechtsman, and M. Segev, Topological Photonic Quasicrystals: Fractal Topological Spectrum and Protected Transport, Phys. Rev. X **6**, 011016 (2016).
[50] C. Lin, P. J. Steinhardt, and S. Torquato, Light Localization in Local Isomorphism Classes of Quasicrystals, Phys. Rev. Lett. **120**, 247401 (2018).
[51] J. E. S. Socolar, P. J. Steinhardt, and D. Levine, Quasicrystals with arbitrary orientational symmetry, Phys. Rev. B **32**, 5547 (1985).
[52] V. Popescu and A. Zunger, Extracting E versus $\vec{k}$ effective band structure from supercell calculations on alloys and impurities, Phys. Rev. B **85**, 085201 (2012).
[53] P. B. Allen, T. Berlijn, D. A. Casavant, and J. M. Soler, Recovering hidden Bloch character: Unfolding electrons, phonons, and slabs, Phys. Rev. B **87**, 085322 (2013).
[54] H. Nishi, Y.-I. Matsushita, and A. Oshiyama, Band-unfolding approach to Moiré-induced band-gap opening and Fermi level velocity reduction in twisted bilayer graphene, Phys. Rev. B **95**, 085420 (2017).
[55] A. I. Goldman and R. F. Kelton, Quasicrystals and crystalline approximants, Rev. Mod. Phys. **65**, 213 (1993).
[56] C. Janot, *Quasicrystals. A Primer 2nd* (Clarendon Press, Oxford, 1994), Vol. 30.
[57] K. Wang, S. David, A. Chelnokov, and J. M. Lourtioz, Photonic band gaps in quasicrystal-related approximant structures, J. Mod. Opt. **50**, 2095 (2003).
[58] See Supplemental Material at http://link.aps.org/supplemental/10.1103/PhysRevLett.127.043901 for (1) the generation of supercell of quasicrystals, (2) spectral weight of band-unfolding scheme, (3) numerical methods used to calculate eigenmode, far-field polarization states and Q factor, (4) multipolar expansions, (5) point-group symmetry of eightfold quasicrystal and empty-lattice bands, (6) cluster model of the octagonal quasicrystals, (7) extraction of polarization vector fields from experimental data, and (8) results of freestanding photonic quasicrystal slabs, which includes Refs. [60,61].
[59] J. E. S. Socolar, T. C. Lubensky, and P. J. Steinhardt, Phonons, phasons, and dislocations in quasicrystals, Phys. Rev. B **34**, 3345 (1986).
[60] A. Gelessus, Character tables for chemically important point groups, https://symmetry.jacobs-university.de.
[61] S. M. Lubin, A. J. Hryn, M. D. Huntington, C. J. Engel, and T. W. Odom, Quasiperiodic Moiré plasmonic crystals, ACS Nano **7**, 11035 (2013).

[62] Z. Sadrieva, K. Frizyuk, M. Petrov, Y. Kivshar, and A. Bogdanov, Multipolar origin of bound states in the continuum, Phys. Rev. B **100**, 115303 (2019).
[63] J. D. Jackson, *Classical Electrodynamics*, 3rd ed. (Wiley, New York, 1999).
[64] P. Grahn, A. Shevchenko, and M. Kaivola, Electromagnetic multipole theory for optical nanomaterials, New J. Phys. **14**, 093033 (2012).
[65] P. J. Steinhardt, H. C. Jeong, K. Saitoh, M. Tanaka, E. Abe, and A. P. Tsai, Experimental verification of the quasi-unit-cell model of quasicrystal structure, Nature (London) **396**, 55 (1998).
[66] S. I. Ben-Abraham and F. Gähler, Covering cluster description of octagonal MnSiAl quasicrystals, Phys. Rev. B **60**, 860 (1999).
[67] E. Abe, Y. Yan, and S. J. Pennycook, Quasicrystals as cluster aggregates, Nat. Mater. **3**, 759 (2004).
[68] E. L. Ivchenko and G. Pikus, *Superlattices and Other Heterostructures: Symmetry and Optical Phenomena* (Springer Science & Business Media, Berlin, 2012), Vol. 110.
[69] V. M. Agranovich and V. Ginzburg, *Crystal Optics with Spatial Dispersion, and Excitons* (Springer Science & Business Media, Berlin, 2013), Vol. 42.
[70] K. Sakoda, *Optical Properties of Photonic Crystals* (Springer Science & Business Media, Berlin, 2004), Vol. 80.
[71] Z. Xiong, Q. Yang, W. Chen, Z. Wang, J. Xu, W. Liu, and Y. Chen, On the constraints of electromagnetic multipoles for symmetric scatterers: eigenmode analysis, Opt. Express **28**, 3073 (2020).
[72] S. Gladyshev, K. Frizyuk, and A. Bogdanov, Symmetry analysis and multipole classification of eigenmodes in electromagnetic resonators for engineering their optical properties, Phys. Rev. B **102**, 075103 (2020).
[73] C. Huang, C. Zhang, S. Xiao, Y. Wang, Y. Fan, Y. Liu, N. Zhang, G. Qu, H. Ji, J. Han, L. Ge, Y. Kivshar, and Q. Song, Ultrafast control of vortex microlasers, Science **367**, 1018 (2020).
[74] Z. Zhang, X. Qiao, B. Midya, K. Liu, J. Sun, T. Wu, W. Liu, R. Agarwal, J. Jornet, S. Longhi, N. Litchinitser, and L. Feng, Tunable topological charge vortex microlaser, Science **368**, 760 (2020).
[75] D. Varjas, A. Lau, K. Pöyhönen, A. R. Akhmerov, D. I. Pikulin, and I. C. Fulga, Topological Phases without Crystalline Counterparts, Phys. Rev. Lett. **123**, 196401 (2019).
[76] C. W. Peterson, T. Li, W. Benalcazar, T. Hughes, and G. Bahl, A fractional corner anomaly reveals higher-order topology, Science **368**, 1114 (2020).